College of Engineering

Encyclopedia of Materials Science and Technology, Eds. Buschow, Cahn, Flemings, Kramer, Mahajan and Veyssiere, Elsevier Science 2004.

Mechanical Properties of the MAX Phases

By now it is fairly well established that the layered ternary carbides and nitrides with the general formula $M_{n+1}AX_n$ (MAX), where $n = 1$, 2, or 3, M is an early transition metal, A is an A-group element (mostly IIIA and IVA), and X is either C or N, represent a new class of solids (Barsoum 2000, Barsoum and El-Raghy 2001a). These phases are layered with $M_{n+1}X_n$ layers interleaved with layers comprised of pure hexagonal nets of the A-group element. The $M_{n+1}AX_n$ unit cells—space group $P6_3/mmc$—have two formula units per unit cell. There are roughly 50 M_2AX phases (Nowotny 1970); three M_3AX_2 (Ti_3SiC_2 (Jeitschko and Nowotny 1967), Ti_3GeC_2 (Wolfsgruber *et al.* 1967), and Ti_3AlC_2 (Pietzka and Schuster 1994)), and one M_4AX_3 namely, Ti_3AlN_4 (Barsoum *et al.* 1999a, Rawn *et al.* 2000). Mainly as a result of the way they deform (Fig. 1), they have been labeled polycrystalline nanolaminates (Barsoum *et al.* 1997).

The $M_{n+1}AX_n$ phases combine an unusual, and sometimes unique, combination of properties (Barsoum 2000). Like their corresponding binary carbides and nitrides, they are elastically stiff, have relatively low thermal expansion coefficients, good thermal and electrical conductivities, and are resistant to chemical attack. As this entry will show, however, mechanically they cannot be more different: they are relatively soft (1–5 GPa) and most readily machinable, thermal shock resistant, and damage tolerant. Moreover, some are fatigue and creep, and oxidation resistant. At higher temperatures, they go through a ductile-to-brittle transition. At room temperature, they can be compressed to stresses as high as 1 GPa and fully recover upon removal of the load, while dissipating 25% of mechanical energy (Barsoum *et al.* 2003).

This entry summarizes our current understanding of the mechanical properties of the $M_{n+1}AX_n$ phases, with emphasis on Ti_3SiC_2, which is the most studied and best understood to date. However, based on limited results on other phases there is little doubt that what applies to Ti_3SiC_2 applies to the other $M_{n+1}AX_n$ phases as well. A more complete review of their atomic structure and physical properties such as elastic moduli, electrical and thermal properties, etc., appears in the article *Physical and Chemical Properties of the MAX Phases*.

To understand the response of the $M_{n+1}AX_n$ phases to stress, it is imperative to understand the nature of their dislocations and concomitant slip systems.

1. Atomistics of Deformation

1.1 Dislocation and Defects in the $M_{n+1}AX_n$ Phases

The key to understanding the mechanical properties of the $M_{n+1}AX_n$ phases is the fact that only basal plane dislocations exist. These dislocations are mobile and multiply, even at temperatures as low as 77 K. Transmission electron microscopy (TEM) (Farber *et al.* 1998, Barsoum *et al.* 1999b) and high-resolution transmission electron microscopy (HRTEM) (Farber *et al.* 1998, 1999) studies of Ti_3SiC_2 revealed the presence of only perfect dislocations lying in the basal planes with a Burgers vector $\boldsymbol{b} = \frac{1}{3}\langle 11\bar{2}0\rangle$ or 1.54 Å in length. Every dislocation is of a mixed nature with an edge and screw component (Farber *et al.* 1999, Kooi *et al.* 2003).

Because they are confined to the basal planes, the dislocations arrange themselves either in arrays (pile-ups) on the same basal planes (Fig. 2(a)), or in walls (low- and high-angle grain boundaries) normal to the basal planes (Fig. 2(a)). The walls have both tilt and twist components (Farber *et al.* 1999, Kooi *et al.* 2003).

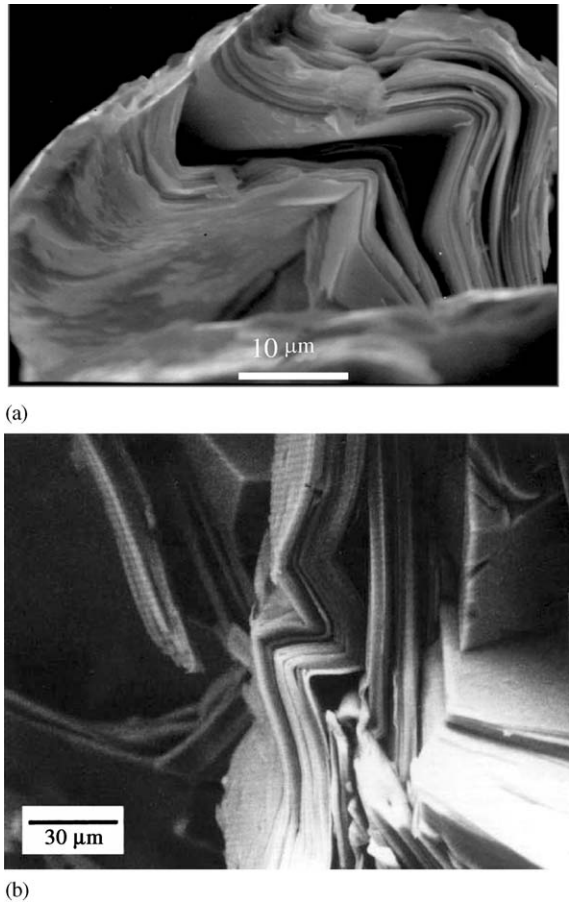

Figure 1
Typical examples of the nanolaminated nature of the MAX phases. SEM micrographs of: (a) a Ti_3SiC_2 surface scribed with a sharp point and (b) typical kinking and delaminations observed on fractured surfaces of Ti_3SiC_2.

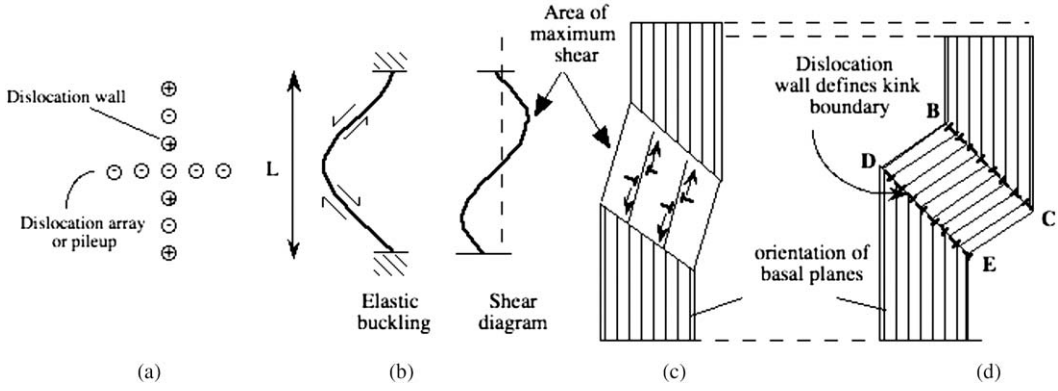

Figure 2
Schematic of (a) dislocation walls (vertical) and arrays or pile-ups (horizontal) in the MAX phases. Both are confined to the basal planes. The + and − signs denote the orientations of the screw dislocations in the wall (Farber *et al.* 1998). (b) Elastic buckling and corresponding shear diagram, and (c) initiation of pairs of dislocations in areas of maximum shear. (d) KB and kink boundaries comprised of edge dislocations of one sign giving rise to the classic stove-pipe shape.

To account for both, the boundary was interpreted to be composed of parallel, *alternating*, mixed perfect dislocations with two different Burgers vectors lying in the basal plane at an angle of 120° relative to one another. The boundary twist was provided for by having an excess of one type of dislocation (Farber *et al.* 1999, Kooi *et al.* 2003).

Dislocation interactions, other than orthogonal (Fig. 2(a)), are very unlikely to occur, and have not been reported to date. As discussed later this fact has very far-reaching ramifications in that substantial deformation can now occur without work hardening in the classic sense. Given that nonbasal dislocations would have Burgers vectors $> c$ (viz. > 11–23 Å), their presence is highly unlikely. Furthermore, as a result of their high c/a ratios, twinning is unlikely (Hess and Barrett 1949).

In addition to dislocations, stacking faults were also observed (Farber *et al.* 1998). The stacking faults are typically growth defects where locally an Si plane is missing and the stacking twin symmetry broken such that thin lamella with an $M_{n+1}X_n$ chemistry remain with identical stacking as [111] in the rock salt structure (Yu *et al.* 2003, Kooi *et al.* 2003). All stacking faults and their bounding dislocations also lie in basal planes with their displacement vectors parallel to [0001] (Faber *et al.* 1998, Yu *et al.* 2003). Grain boundaries are another planar defect present in polycrystalline samples, but their structure is still largely an open question.

1.2 Deformation Mechanisms

The key mechanism without which the deformation of the $M_{n+1}AX_n$ phases cannot be understood is the formation of kink bands (KBs). It is therefore important to briefly review what is known about KBs. KBs in crystalline solids were first observed in Zn single crystals loaded parallel to their basal planes (Orowan 1942). Later, Hess and Barrett (1949) proposed a model to explain their formation by the regular glide of dislocations. Initially, upon loading of a long, thin column of length L, elastic bending creates maximum shear stresses—assuming perfect symmetry—at $L/4$ and $3L/4$ (Fig. 2(b)). Above a critical value this shear stress is sufficient to create, within the volume that is eventually to become the KB, a pair of dislocation walls of opposite signs that move in opposite directions (Fig. 2(c)). The end result is two regions of severe lattice curvature, separated from each other and from the unkinked crystal by well-defined kink boundaries BC and DE (Fig. 2(d)).

Note that KBs are expected only in crystals that do not twin, such as hexagonal metals or alloys having an axial c/a ratio greater than ≈ 1.73 (Hess and Barrett 1949). With c/a ratios that vary from 3 to 7, it is not surprising that $M_{n+1}AX_n$ phases deform by this mechanism.

The Hess and Barrett model was qualitative; a few years later Frank and Stroh (1952) proposed a more quantitative model in which pairs of dislocations of opposite sign nucleate and grow at the tip of a thin elliptical kink with dimensions, α and β, such that $\alpha \gg \beta$ (Fig. 3(a)). The precise mechanism responsible for nucleation of kinks has, to date not been identified. However, by assuming the local stress needed to form a dislocation pair to be $\approx G/30$, where G is the shear modulus, Frank and Stroh (1952) showed that at a critical kinking angle, $\gamma_c \approx 5$–$6°$, the dislocation walls will grow rapidly until they meet a grain boundary (interior grains) or surface (exterior

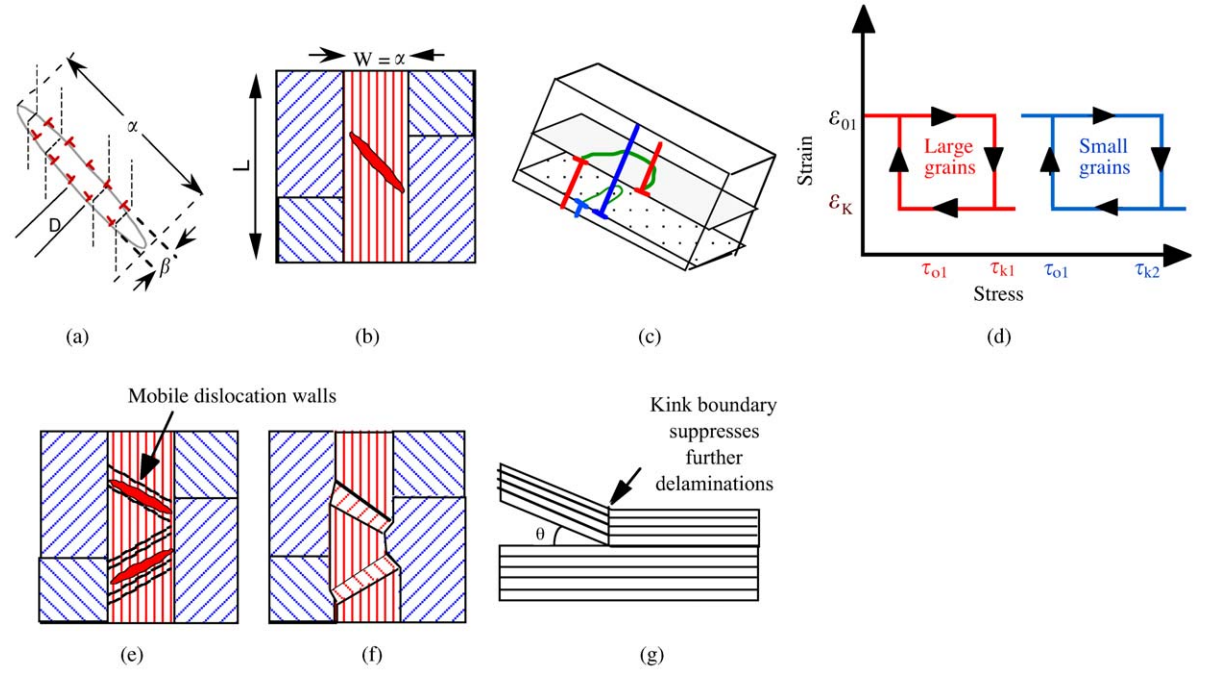

Figure 3
Schematic representation of: (a) thin elliptic cylinder with axes α and β and $\alpha \gg \beta$. The sides are comprised of two dislocation walls (shown in red) of opposite sign, and uniform spacing D. (b) Formation of an IKB in hard (red) grains adjacent to soft (blue) grains. The lines in the grains denote basal planes. At this stage it is fully reversible. (c) Three-dimensional representation of two pairs of dislocations in a wall, emphasizing the dislocation loop and how it can extend along the basal planes unimpeded. (d) Hysteretic element associated with IKBs based on Eqn. (1). Below a certain stress, τ_k, that depends on grain size, the IKB is energetically unfavorable and does not nucleate. Upon removing the load, friction associated with the dislocation lines ensures that the IKB will not collapse until a stress $\tau_0 < \tau_k$. (e) Multiple pile-ups and kink bands in a large grain. Dotted lines denote walls that have separated from the source and are moving away from it. This only happens at higher temperatures and/or stresses. (f) Same as (d) after removal of stress, emphasizing formation of grain boundaries (dark lines). (g) Schematic of a delaminating grain showing how a kink boundary can suppress further delamination.

grains). In other words, the formation of an incipient kink band (IKB)—like the growth of a crack—is autocatalytic and sudden. The critical remote shear stress, τ_c, needed to convert a subcritical kink into an IKB—i.e., render the former unstable—will depend on α, and is given by

$$\tau_c \approx \sqrt{\frac{G^2 b\gamma}{\alpha}} \qquad (1)$$

The most important ramification of Eqn. (1) is that the smaller the domain size α, or the volume available for the creation of an IKB, the larger the stresses required. Mechanistically, or phenomenologically, the response to stress of a grain in which an IKB forms is shown in Fig. 3(d); it will only kink when the applied shear stress $\tau_{ki} > \tau_c$ is given by Eqn. (1). Once it kinks, the domain or grain shrinks by a strain ε_{ki}. When the stress is reduced the friction associated with the dislocation lines will ensure that the IKB disappears at a stress $\tau_o < \tau_c$ (Fig. 3(d)). Since τ_c depends on α, finer-grained samples will form IKBs at higher stresses than coarse-grained samples. IKBs are thus the key microstructural hysteretic element.

In the Frank and Stroh analysis, it was assumed that once an IKB nucleated it would immediately extend to a free surface, eliminating the mutual attraction and resulting in two parallel, mobile noninteracting dislocation walls (i.e., Fig. 3(e)). It is the repetition of this process that results in the generation of new dislocation walls whose coalescence form the kink boundaries (Fig. 3(f)). The idea that an IKB can reach a grain boundary and not dissociate (Fig. 3(b)) was not considered; as discussed below, it is crucial. At this juncture it is worth noting that direct TEM evidence for the presence of parallel

dislocation walls and associated lattice rotations has been reported (Barsoum *et al*. 1999b, Molina-Aldareguia *et al*. 2003).

Delaminations in layered solids—from fiber composites to geologic strata—in many critical situations can lead to catastrophic failure. Therefore, the role KBs play in suppressing delaminations in the $M_{n+1}AX_n$ phases is both scientifically and technologically of vital importance. To best appreciate how KBs suppress delaminations, consider the schematic shown in Fig. 3(g), depicting the top portion of a grain—whose basal planes lie parallel to the surface—being pulled upwards, or normal to the basal planes. In most layered material, once a delamination crack, such as shown in Fig. 3(g), is initiated it takes little energy to further separate the two sections from each other. In the $M_{n+1}AX_n$ phases, on the other hand, these delaminations only proceed part way before they are totally suppressed (see below). This comes about because delaminations with kink boundaries at their end can only advance if the *entire* wall or kink boundary also moves; an energetically very expensive proposition that gets more expensive as the angle θ in Fig. 3(g) becomes steeper (Barsoum and El-Raghy 1999, Barsoum *et al*. 1999b, Radovic *et al*. 2003). Said otherwise, the remarkable damage tolerance of the $M_{n+1}AX_n$ phases discussed below is built in their deformation mechanism at the atomic level. These solids may not be self-healing, but they are damage tolerant at the nanolevel.

Dislocation arrays (Farber *et al*. 1998, 1999, Barsoum *et al*. 1999b) also play a critical role. At this stage their role is less clearly understood than that of the walls. However, delaminations are most likely to occur at the intersection of the dislocation walls and arrays (Stroh 1954, 1958, Barsoum *et al*. 1999b, Kooi *et al*. 2003), eliminating the latter and resulting in large strain energy releases. Note that the arrays are also inherent to the overall kinking process; without them, the various lamellae cannot shear relative to each other; the precursor for all that follows (Barsoum *et al*. 1999b). The stresses at the tips of arrays could also nucleate IKB in adjacent grains. It is also not unreasonable to assume that, if present, ahead of an IKB, they would create a strong driving force for delaminations to occur at the plane in which they exist. Lastly, there is also little doubt that they are responsible for the large internal stresses that develop in these materials as a result of loading.

1.3 Plastic Anisotropy and Internal Stresses

The $M_{n+1}AX_n$ phases, e.g., ice, graphite, and layered minerals such as mica, are plastically very anisotropic. This plastic anisotropy, combined with the fact that they lack the five independent slip systems needed for ductility, quickly lead to a very uneven state of stress when a polycrystalline sample is loaded (Duval *et al*. 1983). Glide of basal plane dislocations takes place only in favorably oriented or soft grains, which rapidly transfers the load to hard grains, viz. those not favorably oriented to the applied stress. Needless to say, this leads to high internal stresses. Interestingly enough, and not coincidentally, the hard grains are those that are most prone to buckling or kink banding. In compression, grains whose *c*-axes are normal to the applied load will kink, whereas in tension, those for which the *c*-axes are parallel. Note elastic anisotropy is not a necessary requirement for kinking; Ti_3SiC_2 is elastically quite isotropic (Holm *et al*. 2001).

All $M_{n+1}AX_n$ phases tested to date go through a brittle-to-ductile transition. The most important clue as to what is occurring above the transition temperature is the fact that the fracture toughness, K_{1C}, actually *decreases* (Chen *et al*. 2001), in contradistinction to almost all other crystalline solids. Such a decrease not only rules out the activation of other slip systems, but just as importantly, indicates that the back-pressure from dislocation arrays at the crack tip is reduced. The most likely mechanism for this to occur is for delaminations and/or grain boundary decohesion to occur. In other words, the only assumption one need make to understand the high-temperature response of the $M_{n+1}AX_n$ phases is a temperature-dependent grain boundary decohesion stress and/or a delamination stress.

At this juncture all the elements needed to understand the response of the $M_{n+1}AX_n$ phases to stress are in place. The following section deals with ambient temperature results including thermal shock; the latter parts deal with the effect of temperature on the mechanical properties and other facets of the mechanical properties of the $M_{n+1}AX_n$ phases.

2. Room Temperature Response

2.1 Compression Behavior of Quasi-single Crystals and Polycrystals

When highly oriented, quasi-single crystals macrograined ($\approx$2 mm in diameter) samples of Ti_3SiC_2 are tested in compression the response is anisotropic (Barsoum and El-Raghy 1999). When the basal planes are oriented in such a way that allows for slip (*x*-direction in inset in Fig. 4(a)) the samples yield at $\approx$200 MPa (Fig. 4(a)) and the deformation occurs by the formation of shear bands (not shown). By contrast, when the slip planes are parallel to the applied load (*z*-direction in inset in Fig. 4(a)), and deformation by ordinary dislocation glide is impossible, the stress–strain curves show clear maxima at stresses between 230 MPa and 290 MPa, followed by a region of strain softening and finally recovery (Fig. 4(a)). Here, the deformation occurs by a

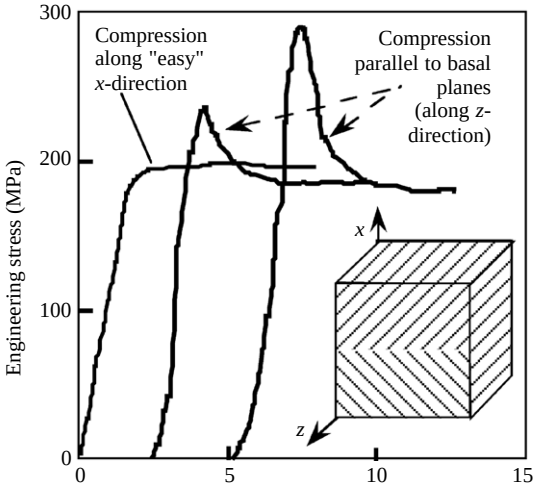

(a)

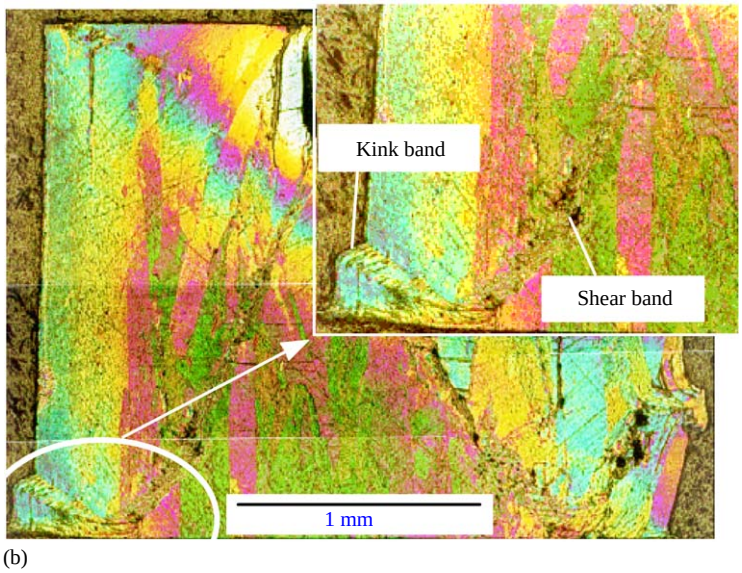

(b)

Figure 4
(a) Engineering stress–strain curves of 2 mm cubes of highly oriented samples of Ti_3SiC_2. Inset shows schematic of cube and basal plane orientations. (b) Optical OM micrograph of polished and etched sample after deformation parallel to the basal planes. Note kinking at corners. Inset shows a higher magnification view of lower left corner emphasizing the kink band and, as importantly, the genesis of the shear band that cuts across the cube face (Barsoum and El-Raghy 1999).

combination of KB formation at the corners of the tested cubes, delaminations within individual grains, and ultimately shear band formation (Fig. 4(b)). Note the KB visible on the bottom left-hand side of the cube in Fig. 4(b) did *not* result in the total delamination of the outermost grain in which it was initiated. This observation was taken to be the first compelling microstructural evidence that KBs are potent suppressors of delamination (Barsoum and El-Raghy 1999).

Polycrystalline samples of Ti_3SiC_2 subjected to compressive loads and temperatures up to $\approx 900\,^{\circ}C$ fail in a quasi-brittle manner by shearing, roughly at 45° to the loading axis. Not all MAX phases fail suddenly; actually most exhibit graceful failure characteristics in that the stress–strain curves are

closer to an inverted shallow V, than a sharp drop at a maximum stress (Barsoum *et al.* 2000, Tzenov and Barsoum 2000). The failure mode is still shear failure across a plane, but presumably enough ligaments reach across the plane to result in a less sudden loss in load bearing capability. This tendency increases with increasing grain size and reduced loading rates.

2.2 IKBs and Kinking Nonlinear Elastic (KNE) Solids

The strongest evidence for the formation of IKBs is the fully reversible nature of the deformation observed when bulk Ti_3SiC_2 samples are loaded in compression (Barsoum *et al.* 2003) and recent nanoindentation results (Murugaiah *et al.* 2004). The room temperature stress–strain curves of macroscopic polycrystalline cylinders of Ti_3SiC_2 outline fully reversible, reproducible, closed loops whose size, shape, and slopes depend on grain size, but not strain rate (Fig. 5(a)). In this article, reference will be made mostly to two different microstructures, fine- (3–5 μm) and coarse-grained (plate-like grains, 50–200 μm in diameter and 5–20 μm thick). Fine-grained (3–5 μm) samples can be compressed to stresses up to 1 GPa and fully recover upon the removal of the load (inset in Fig. 5(a)). In one case, a sample was cycled 100 times at 700 MPa, with no apparent difference between the first and last cycles (Barsoum *et al.* 2003).

The fully reversible deformation, its strong dependence on grain size but not strain rate, the propensity of the MAX phases to form KBs, and the fact that the energy dissipated per cycle, W_d, increases with the square of the applied stress (Fig. 5(b)) provide compelling, almost irrefutable, evidence for the formation of IKBs (Barsoum *et al.* 2003). Assuming τ in Eqn. (1) to be $\approx G/1000$ (for Ti_3SiC_2 $G = 130$ GPa), $\gamma = 5^\circ$, yields a value of α of ≈ 10 μm. It is thus not surprising that at ≈ 250 MPa, the elastic strain contributions to the total strain of the FG samples (with grains in the 3–5 μm range) is much higher than the corresponding values for the CG samples in which large hexagonal plate-like grains with diameters of 100–300 μm and ≈ 10 μm thick are embedded in a fine-grained matrix (Fig. 5(a)). In other words, the CG samples would rather form IKBs than elastically linearly deform.

The room temperature loss factors ($W_d/2\pi$) for Ti_3SiC_2 are exceedingly high and are probably a record for crystalline solids. They are several orders of magnitude higher than those of other structural ceramics, higher than most woods, and comparable to polypropylene and nylon (Fig. 6). These high values (0.7 MJ m^{-3} at 1 GPa) are consistent with a solid in which no work hardening—in the classic sense—is occurring. In other words, because the dislocation lines are confined to the basal planes (Fig. 3(c)), they cannot entangle and thus can move to and fro over distances that are significantly higher than those in other solids. It is important to note here that in contrast to most other crystalline solids—with the notable exception of graphite—W_d is proportional to σ^2 (Fig. 5(b)).

Recent nanoindentation work with a 13.5 μm spherical indenter (Murugaiah *et al.* 2004) on individual Ti_3SiC_2 grains offers further compelling evidence that IKBs form at the grain level. Unlike the nanoindentation response of crystalline materials that almost always results in plastic deformation and/or damage, Ti_3SiC_2 can be loaded up to stresses of ≈ 10 GPa, deform plastically and then recover upon unloading to such an extent that the indentations *cannot* be found. In that respect it is not unreasonable to think of the $M_{n+1}AX_n$ phases as behaving as dislocation-based elastomers, in that they can be loaded repeatedly, without damage, and dissipate significant amounts of energy during each cycle.

Here again—but this time because of the confined nature of the deformation to much higher stresses—the load–displacement curves trace almost fully reversible loops that are a function of grain orientation. At low loads, fully reversible *closed* loops are obtained for the same reasons outlined above. At intermediate loads (10–200 mN) the first loop is slightly open, but then all subsequent loops obtained from the same location taken to the same stress are not only closed, but, as important, *harder* than the first (Fig. 7). The hardening observed is key because it rules out microcracking. (Phase transitions have not been observed and can be ruled out.)

The simplest explanation for this observation is that at sufficiently high σ's the walls comprising the IKB split, become mobile and move away from the source, accounting for the small plastic deformation recorded during the first loadings. On subsequent loading the presence of these walls obviously hardens the indented area. At high stresses, the mobile dislocation walls will create KBs that reduce α and thus increase the stress at which new IKBs form. Direct evidence for this "grain refinement" can be found in nanoindentation studies on single crystals of graphite (Barsoum *et al.* 2004a). The area under the indenter breaks up into submicron grains that are quite resistant to deformation. The same occurs in mica (Barsoum *et al.* 2004b).

When the nanoindentation results are converted to stress–strain curves, W_d calculated and plotted on the same log–log plot as the bulk results, excellent agreement between the two sets of data is obtained (Fig. 5(b)). This clearly implies that the same physics is occurring at the different length scales. Note here, because the deformation is confined, the values of W_d are of the order of 10 GJ m^{-3}

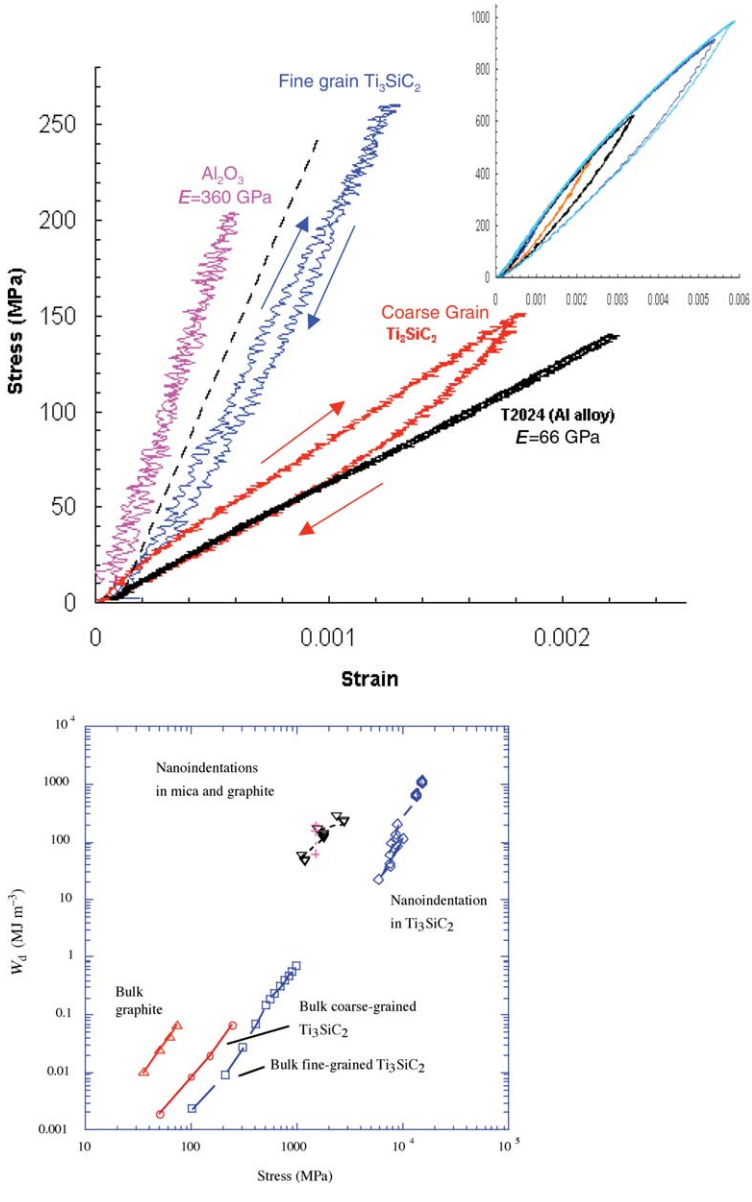

Figure 5
(a) Stress–strain curves for FG- and CG-grained Ti_3SiC_2. Dotted line is linear elastic response expected for Ti_3SiC_2 had kinking *not* occurred. The loop labeled coarse-grained Ti_3SiC_2 represents three loading and unloading cycles that differed from each other by a factor of 10 in loading and unloading rates. The reproducibility is noteworthy. Also included are the results on Al_2O_3 and Al for comparison. Inset shows successive loops obtained as the stress was increased up to 1 GPa. Note all loading curves are identical (Barsoum *et al.* 2003). (b) log–log W_d vs. σ plot. The results in the lower left hand corner are for bulk samples; those in the upper right from nanoindentations (Murugaiah *et al.* 2004).

(Fig. 5(b)) and the expected W_d versus $\approx\sigma^2$ relationship is valid over 6 orders of magnitude of W_d. Also plotted in Fig. 5(b) are results on graphite and mica, that, together with the MAX phases, and nonlinear mesoscopic solids, NMEs (Guyer *et al.* 1995) layered silicates and oxides, belong to a much larger class of solids—KNE solids—that deform by kinking (Barsoum *et al.* 2004b).

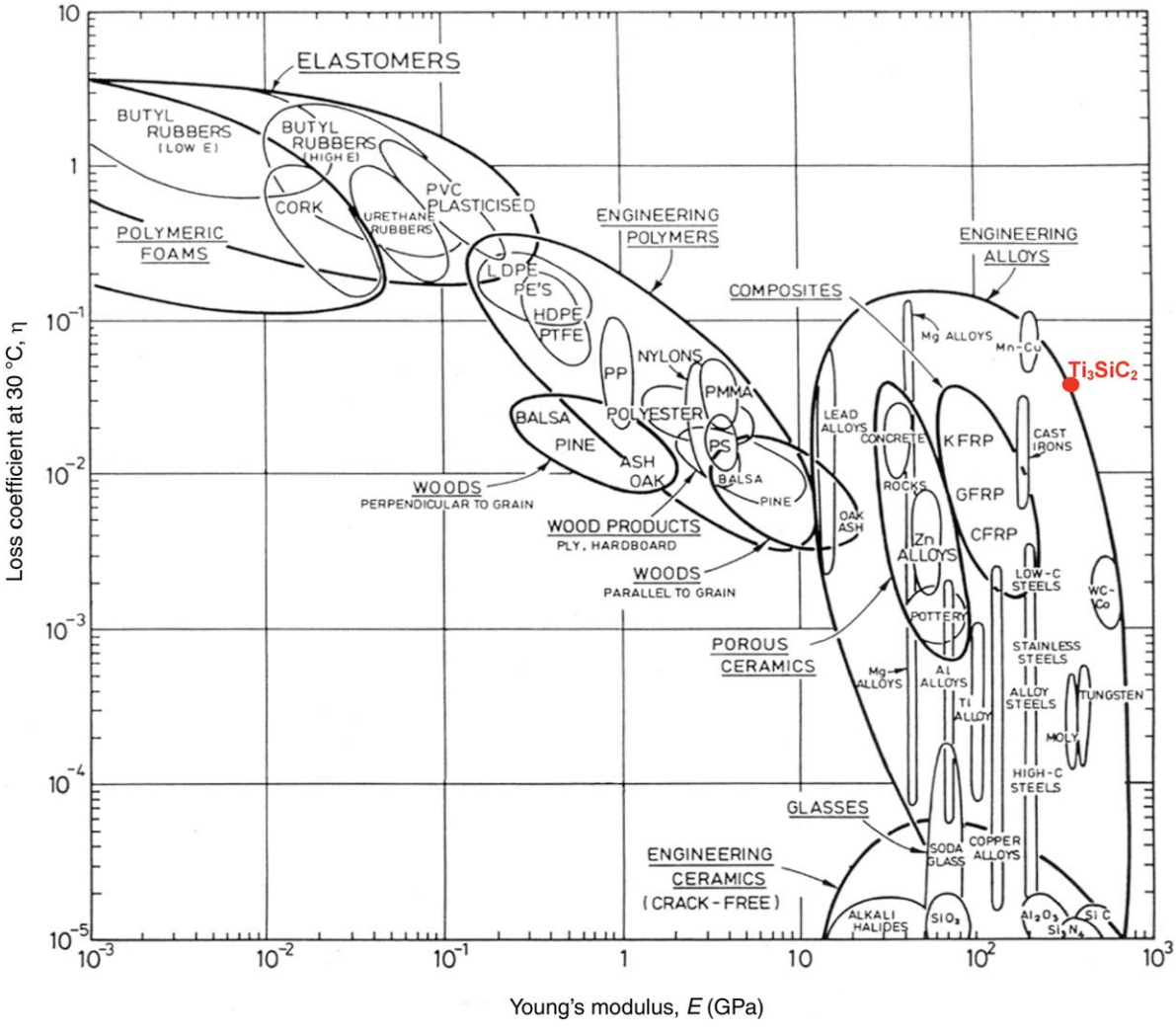

Figure 6
Ashby-map of loss factor defined as $W_d/2\pi$ vs. Young's modulus (Ashby 1989).

The transformation of the IKB into two mobile walls must be accompanied by the formation of a free surface either at a grain boundary, or, much more likely in this case, one that forms by delaminations. For graphite single crystals, it is the latter (Murugaiah *et al.* 2004). Note that direct TEM evidence for the formation of kink bands under Berkovich indenters has recently been published (Kooi *et al.* 2003, Molina-Aldareguia *et al.* 2003).

2.3 Hardness and Damage Tolerance

The $M_{n+1}AX_n$ phases, unlike the MX carbides, are relatively soft and exceedingly damage tolerant. The hardness values of polycrystalline $M_{n+1}AX_n$ phases fall in the relatively narrow range of 1–5 GPa. They are thus softer than most structural ceramics, but harder than most metals (Barsoum 2000). The low hardness persists—at least in Ti_3SiC_2—even at temperatures as low as 77 K (Kuroda *et al.* 2001).

Working with CVD single crystals, Nickl *et al.* (1972) were the first to note that the hardness of Ti_3SiC_2 was anisotropic and higher when loaded along the *c*-direction. This was later confirmed by Goto and Hirai (1987), who also were the first to show that the hardness was a function of indentation load. Both observations are characteristic of the MAX phases (Barsoum 2000). With decreasing load, the hardness increases (Fig. 8, top curve) and below a

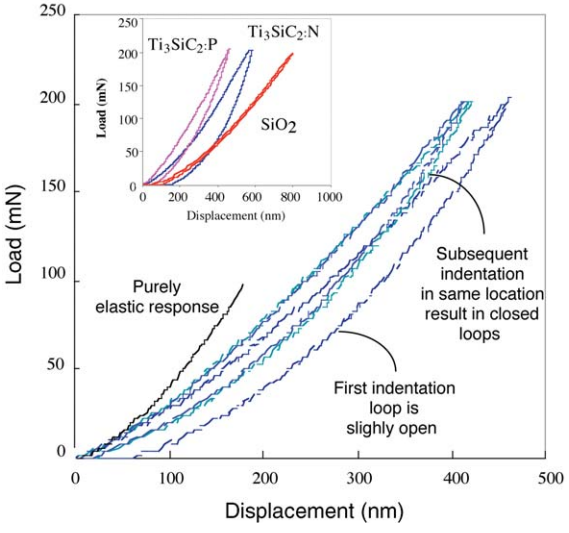

Figure 7
Typical load vs. depth-of-indentation response of a Ti_3SiC_2 surface for which the basal planes were: perpendicular, or edge-on, to the surface. The loop area associated with the first indentation is larger than subsequent indentations in the same location. Inset compares first loops in both orientations; for the most part, the loop areas and depths of penetration are higher in the orientation for which the basal planes are parallel to the surface (Murugaiah *et al.* 2004).

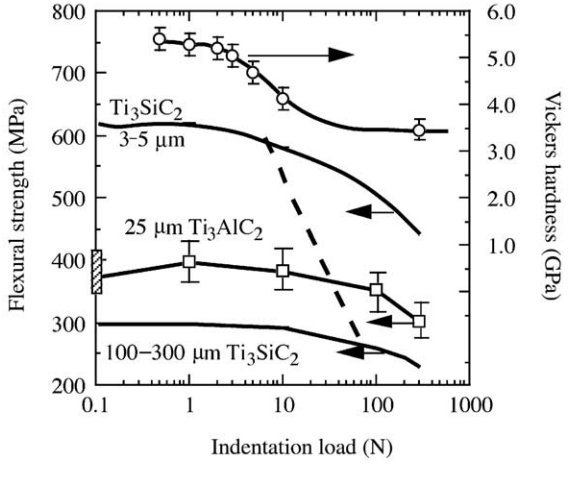

Figure 8
Vickers hardness versus indentation load (top curve): four-point flexural strength vs. indentation loads for fine- and coarse-grained Ti_3SiC_2 and Ti_3AlC_2 with $a \approx 25$ μm grain size. The inclined dashed line is expected behavior for brittle solids (Tzenov and Barsoum 2000).

certain load it is not measurable, since no trace of the indentations is found. These observations were not understood until the recent nanoindentation work in which the reversible nature of the IKBs was elucidated (see above).

Not surprisingly, given their plastic anisotropy, the response to nanoindentations is anisotropic; when the basal planes are parallel to the surface, the extent of plastic deformation is higher than if the basal planes are loaded edge-on (inset in Fig. 7) (Kooi *et al.* 2003, Murugaiah *et al.* 2004). In the former case, it is easier to form KBs because the top surface is unconstrained (Kooi *et al.* 2003, Murugaiah *et al.* 2004).

The damage tolerance values of Ti_3SiC_2 (El-Raghy *et al.* 1997, 1999) and Ti_3AlC_2 (Tzenov and Barsoum 2000) are best exemplified in Fig. 8 (bottom 3 curves) in which the functional dependencies of post-indentation bend strengths are plotted versus Vickers indentation loads. Clearly, the post-indentation flexural strengths of these ternaries are considerably less dependent on the indentation loads than typical brittle ceramics (dashed line in Fig. 8). Similar to ceramics, however, the damage tolerance of coarse-grained microstructures is superior to finer-grained samples.

Typically, Vickers indentations in brittle solids result in sharp cracks extending from corners of the indents that result in sharp reductions in strengths. As first reported by Pampuch *et al.* (1989, 1993) it is difficult to induce cracks from the corners of Vickers indentation in Ti_3SiC_2. Instead of the formation of cracks, delaminations, kinking of individual grains, grain push-outs and pull-outs are observed in the area around indentations (El-Raghy *et al.* 1997, Procopio *et al.* 2000, Tzenov and Barsoum 2000). In short, the main reason for this damage tolerance is the ability of the MAX phases to contain and confine the extent of damage to a small area around the indentations. The atomistic reasons for this state of affairs were discussed above (e.g., Fig. 3(g)).

The importance of such high damage tolerance cannot be overemphasized since it implies that the $M_{n+1}AX_n$ phases are much more tolerant to processing and service flaws, that are typically quite detrimental to the mechanical properties of brittle solids. This, in turn, should also greatly increase manufacturing yields, since the need for full density is relaxed.

2.4 Thermal Sock Resistance

Another characteristic feature of the MAX phases is their excellent thermal shock resistances (Barsoum and El-Raghy 1996). The response of Ti_3SiC_2 to thermal shock depends on grain size (El-Raghy *et al.* 1999); the post-quench flexural strengths of CG

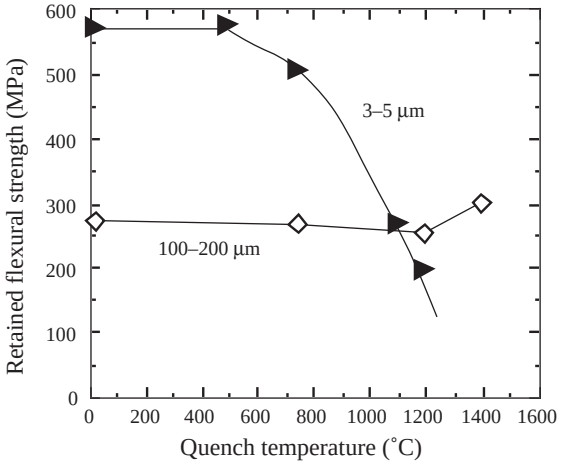

Figure 9
Thermal shock of Ti_3SiC_2 samples with two different grain sizes.

samples are not a function of quench temperature and actually get slightly stronger when quenched from 1400 °C (Fig. 9). The response of fine-grained Ti_3SiC_2 samples is different; instead of exhibiting a critical quenching temperature above which the strength is greatly reduced as typical for ceramics, their post-quenching strengths gradually decrease over a 500 °C range (Fig. 9). The same non-susceptibility to thermal shock is also exhibited by $Ti_3(Si_xGe_{1-x})C_2$ solid solutions (Ganguly *et al.* 2004). In one case, the post-quench flexural strengths of a CG $Ti_3(Si_{0.5}Ge_{0.5})C_2$ sample were actually $\approx$20% *higher* than the as-sintered CG samples (not shown). The reasons for this quench hardening are not entirely clear at this time, but are most probably related to the formation of smaller domains as a result of thermal residual stresses.

2.5 R-curve Behavior and Fatigue

Gilbert *et al.* (2000) reported on the fracture and cyclic fatigue crack growth behavior of Ti_3SiC_2. Both the fine- and coarse-grained microstructures exhibit substantial R-curve behavior—where the stress needed to extend a crack is a function of crack length—at room temperature (Fig. 10(a)). The FG samples initiated at a $K_{1c} \approx 8$ MPa $m^{1/2}$, rising to $\approx$9.5 MPa $m^{1/2}$ after 1.5 mm of crack extension. The CG samples exhibit substantially stronger R-curve behavior, with crack growth initiation between 8.5 MPa $m^{1/2}$ and 11 MPa $m^{1/2}$, and peaking at 14–16 MPa $m^{1/2}$ after 2.7–4 mm crack extension (Fig. 10(a)). The latter value is believed to be one of the highest K_{1c} values ever reported for monolithic, single-phase non-transforming ceramics.

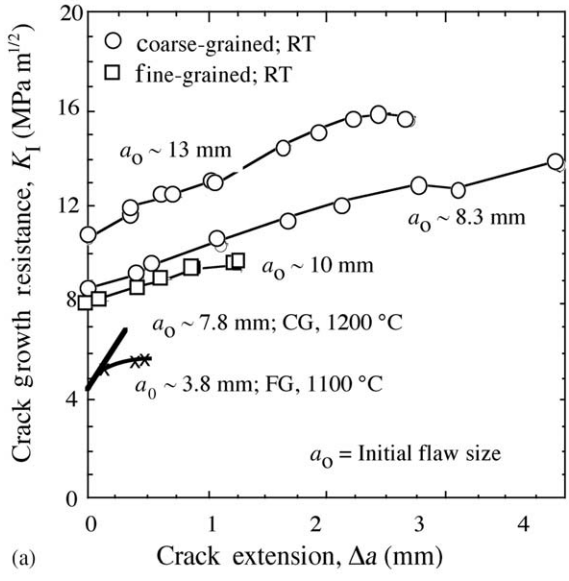

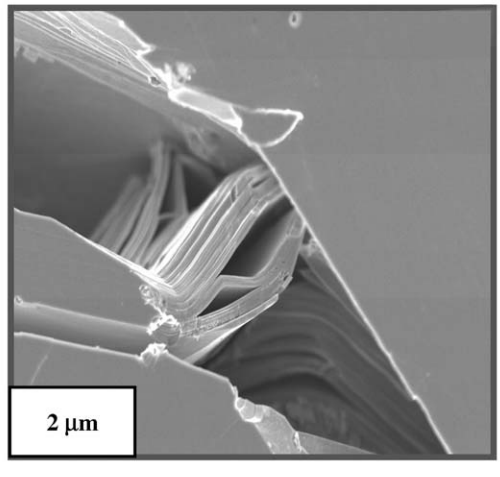

Figure 10
(a) Crack growth resistance, K_R, plotted as a function of crack extension, Δa, for both the fine- and coarse-grained Ti_3SiC_2 microstructures at ambient and elevated temperatures. The initial flaw size, a_0, is indicated for each measured R-curve. Note that K_R drops above the brittle-to-plastic transition temperature (Chen *et al.* 2001). (b) Field-emission SEM image of a bridged crack in the coarse-grained Ti_3SiC_2 microstructure. Heavily deformed lamella bridge the crack, and significant amounts of delamination and bending are observed. Such processes are highly unusual in ceramic systems and must, at least partially, account for the extremely high plateau K_{1C}'s. Crack is growing from left to right (Gilbert *et al.* 2000).

The cyclic fatigue study of coarse- and fine-grained Ti_3SiC_2 samples (Gilbert *et al*. 2000) confirmed a high dependence of cyclic fatigue crack growth rates, da/dN, on the applied stress intensity range, ΔK, that is typical of ceramics. However, the fatigue crack growth thresholds, ΔK_{th}, are comparatively higher than those for typical ceramics and some metals (e.g., 300 M alloy steel) tested under the same conditions. The fatigue threshold of the CG samples (9 MPa $m^{1/2}$) is one of the highest fatigue thresholds ever observed in monolithic, non-transforming ceramics. For the FG structure, the fatigue threshold drops to $\approx$6.5 MPa $m^{1/2}$. With the increase of testing temperature, the fatigue thresholds for both microstructures decrease slightly up to 1100 °C. At 1200 °C which is above the brittle-to-plastic transition (BPT) (see below), the da/dN versus ΔK curves show three distinctive regions that are more pronounced for the FG samples.

Evidence for elastic-ligaments bridging and frictional pull-outs similar to those observed in other structural ceramics were found in all samples after fracture toughness and cyclic-fatigue testing. However, the excellent K_{1c} and K_{th} values can be mostly attributed to the unique KB induced lamellae (Fig. 10(b)) that serve as very tenacious crack bridges, somewhat reminiscent of wood.

3. *High-temperature Response*

All MAX phases tested to date go through a brittle to ductile or BPT. The temperature of the transition varies from phase to phase, but for many Al-containing phases and Ti_3SiC_2, it is between 1000 °C and 1100 °C. The fact that K_{1c} *drops* above the BPT temperature (Fig. 10(a)) (Chen *et al*. 2001) categorically rules out the activation of additional slip systems, which is why it is more accurate to label the transition as a BPT transition, rather than the more common ductile-to-brittle transition. More details on the nature of this transition are discussed below.

3.1 Compressive Properties

Further compelling evidence for the KB-based model discussed above can be found in the high-temperature response of Ti_3SiC_2 to compressive cyclic loadings. Up to $\approx$900 °C, and consistent with the athermal model for the formation of IKBs, there is little change to the shapes or areas of the stress–strain loops in compression (Barsoum *et al*. 2003). At temperatures $>$1000 °C, however, the stress–strain loops are open (Fig. 11(a)) and the response becomes strongly strain rate dependent. Cyclic hardening at temperatures as high as 1200 °C has been observed for both FG (Fig. 11(a)) and CG samples; the effect on the latter, however, is more dramatic (Barsoum *et al*. 2003). The hardening is manifested in two ways: First the areas enclosed by the loops become smaller (Fig. 11(a)). Second, the *initial* slopes of the stress–strain curves approach the linear elastic limit as the number of cycles increase (Fig. 11(a)). The latter clearly implies that the cycling results in microdomains that are harder to kink than the initial grains (i.e., reduction of α in Eqn. (1)).

Along the same lines, and for the same reasons, after cycling at high temperature the room temperature response of the CG samples becomes comparable to those of the FG ones, and the latter approach the linear elastic limit. Figure 11(b) plots room-temperature stress–strain curves of a CG Ti_3SiC_2 sample before and after a 2% deformation at 1300 °C (inset in Fig. 11b). After deformation, the stress-strain loops are distinctly steeper (Zhen *et al*. 2004a). As important, the first loop after deformation, traced in red in Fig. 11(b), is open, but subsequent ones (blue) are closed (Zhen *et al*. 2004a) The simplest interpretation for these observations is that during the first cycle the mobile dislocation walls (Fig. 3(e)) produced at high temperature are swept into the kink boundaries, immobilizing them (Fig. 3(f)). On subsequent loading only IKBs are activated. From these results it is obvious that the deformation at high temperatures effectively reduces the grain size. In other words, the reasons for hardening are similar to the ones invoked to explain hardening under the nanoindenter, namely, the transformation of IKBs to KB, and the reduction in the volume available to form new IKBs.

3.2 Tensile Properties

The response of Ti_3SiC_2 to tensile stresses is a strong function of temperature and strain rate. Below the BPT they are brittle, above they can be quite plastic, with strains to failure up to 25% in some cases, especially at low strain rates (Barsoum *et al*. 2001b) (Fig. 12(a)). The deformation occurs without necking and the majority of the strain at failure is due to damage accumulation in the form of cavitations, pores microcracks, etc. (Radovic *et al*. 2000, 2001, 2002, 2003).

The strain rate sensitivity of $\approx$0.5 (Radovic *et al*. 2000, 2002) determined for both coarse- and fine-grained microstructures of Ti_3SiC_2 is quite high and more characteristic of superplastic solids than typical metals or ceramics. This does not imply, however, that the deformation of Ti_3SiC_2 is in any way similar to that of superplastic solids. The latter have comparable strain rate sensitivities, but only at grain sizes that are at least 2 orders of magnitude smaller than those of the CG Ti_3SiC_2 samples.

3.3 Creep

If the MAX phases are ever to be used as high-temperature structural materials in air, it is critical to understand both their creep behavior and oxidation

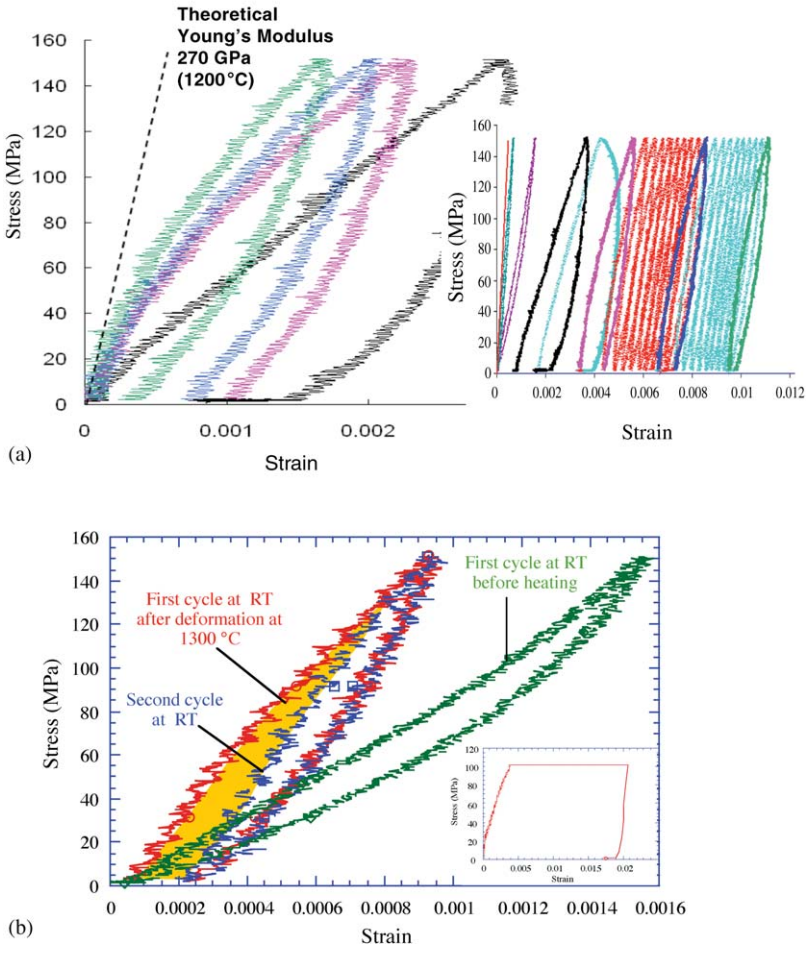

Figure 11
Fine-grain sample of Ti_3SiC_2 cycled in compression at 1200 °C. Inset shows the totality of cycles. Select, color-coded, cycles are extracted from the inset and plotted starting at zero strain for comparison (Barsoum *et al.* 2003). Note the significant cyclic hardening manifested by both reduction in dissipated energy, W_d, and stiffening at low loads. The dashed line is the response predicted for purely elastic deformations. (Barsoum *et al.* 2003). (b) Comparison of the room temperature compressive stress–strain curves of a coarse-grained Ti_3SiC_2 sample tested before and after a 2% deformation at 1300 °C (inset). The latter was loaded twice; the first loading resulted in an open loop, the second and subsequent, only closed loops (Zhen *et al.* 2004a).

resistance. The latter is dealt with separately in another entry.

In the 1000–1300 °C temperature range, Ti_3SiC_2 loaded in tension or compression exhibits primary, secondary, and tertiary creep (Radovic *et al.* 2001, 2003, Zhen *et al.* 2004b). During the short primary creep stage, the deformation rate decreases rapidly. This is followed by a secondary creep regime during which the creep rate, although not truly reaching a constant level, does not change significantly over a wide range. This secondary or minimum creep rate, $\dot{\varepsilon}_{min}$, characterizes a plastic flow in which "hardening" and "softening" are believed to be in dynamic equilibrium.

The $\dot{\varepsilon}_{min}$ for the FG and CG samples in both tension and compression of Ti_3SiC_2 can be described by the following power-law equation (Radovic *et al.* 2001, 2003, Zhen *et al.* 2004b):

$$\dot{\varepsilon}_{min} = \dot{\varepsilon}_0 A \left(\frac{\sigma}{\sigma_0}\right)^n \exp\left(-\frac{Q}{RT}\right) \qquad (2)$$

where A, n, and Q are, respectively, a stress-independent constant, stress exponent, and activation

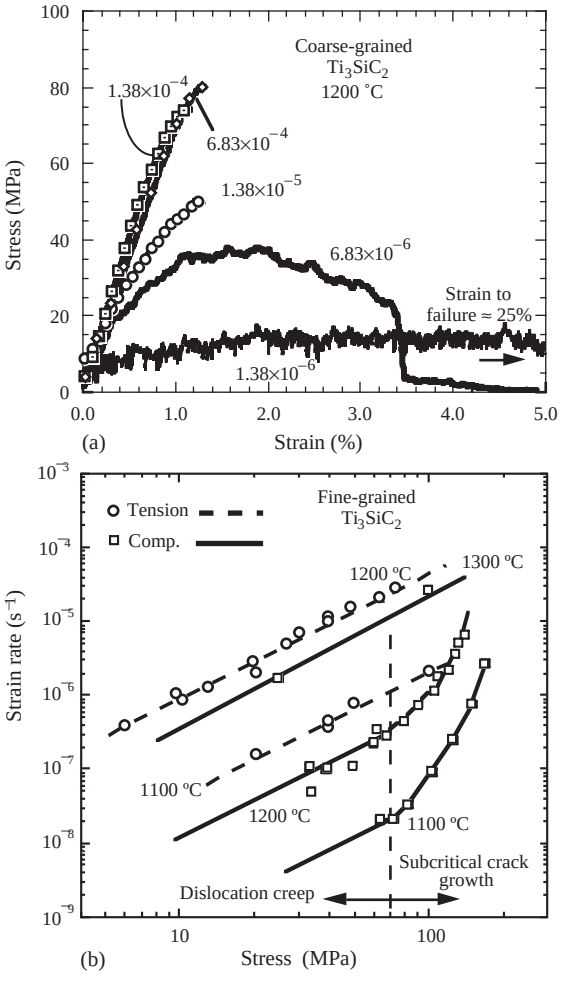

Figure 12
(a) Typical tensile stress–strain curves for coarse-grained Ti_3SiC_2 tested in air at 1200 °C as a function of strain rate. Note strong strain rate sensitivity; at high strain rates, samples are brittle. At low rates, deformations of 25% are possible (Barsoum *et al*. 2001b). (b) Summary of creep response of fine-grained Ti_3SiC_2 tested in tension and compression at various temperatures (Radovic *et al*. 2000, Zhen *et al*. 2004b).

energy for creep. R and T have their usual meanings; $\dot{\varepsilon}_{min} = 1\ s^{-1}$ and $\sigma_0 = 1$ MPa. A summary of the creep results for the FG samples is shown in Fig. 12(b). Table 1 summarizes the values of A, n, and Q obtained.

Based on these, and other results on the mechanical response of Ti_3SiC_2 in the 1000–1300 °C temperature and 10–100 MPa stress ranges, one can conclude the following: (a) Based on the similarities in the values of n, especially at low stresses (Fig. 12(b)), it is fair to conclude that the same mechanism is responsible for the creep of both the FG and CG microstructures. This claim is made despite the differences in activation energies. At this time it is not clear why the latter are a function of type of loading or what their origin is. More work is needed. (b) For both microstructures, at any given temperature, $\dot{\varepsilon}_{min}$ is at least an order of magnitude lower in compression than in tension (Fig. 12(b)). (c) Large internal stresses develop during testing (Radovic *et al*. 2001, 2003, Zhen *et al*. 2004b). The most likely source of these stresses are dislocation pile-ups or arrays. (d) In tension, $\dot{\varepsilon}_{min}$ is a weak function of grain size, with grain size exponents <1. The same is true in compression, but only at low stresses (Fig. 12(b)), which implies that the dominant creep mechanism must be dislocation creep, despite the fact that n is less than the exponents typically associated with dislocation creep (Radovic *et al*. 2001, 2003).

In compression, especially at relatively high stresses and/or temperatures, $\dot{\varepsilon}_{min}$ can actually be *lower* for the FG than the CG microstructures (Fig. 12(b)) (Zhen *et al*. 2004b). In that regime, the stress exponents also become quite large (Fig. 12(b)). The reasons for this unusual phenomenon are not totally understood at this time, but post-testing microstructural examinations of samples in that regime suggest a change in mechanism from dislocation creep to subcritical crack growth. The latter regime is quite difficult to document in tension most likely because the stress state is such as to quickly cause fast fracture. These comments notwithstanding, more work is needed to better understand what is occurring.

At lower stresses, the times to failure measured during tensile creep are considerably longer for the coarse- than for fine-grained microstructures (Radovic *et al*. 2001, 2003). This is attributed to the higher damage tolerance of the CG microstructure, i.e., to the ability of CG structure to sustain higher bridging stresses than the finer ones. Two different bridging mechanisms were observed in creep. The first—in which grains whose basal planes are parallel to the applied load—serves as classic crack bridges. The second mechanism begins with delaminations that are initiated at opposite ends of a single grain, but on different basal planes. With further deformation the torque separates the lamellae between the two delamination cracks to ultimately form crack bridges not unlike the ones shown in Fig. 10(b).

The simplest explanation for these observations, as well as to the fact that K_{1C} actually *decreases* above the PBT, is the following: As in ice (Barsoum *et al*. 2000) and for the same reason, viz. the paucity of operative slip systems, glide of basal plane dislocations takes place only in favorably oriented grains or soft grains. During the short primary creep regime, basal plane dislocations glide and form pile-ups,

Table 1
Summary of creep results for Ti_3SiC_2.

	ln A	n	Q (kJ mol^{-1})	$\dot{\varepsilon}_{min}$ (s)$^{-1}$ at 1200 °C and 50 MPa	Refs.
Compression					
CG	22	2	585 ± 20	2.3×10^{-7}	Zhen *et al.* (2004b)
FG	14	1.9	768 ± 20	2.2×10^{-7}	Zhen *et al.* (2004b)
Tensile					
CG	17	2	458 ± 12	3.5×10^{-6}	Radovic *et al.* (2003)
FG	19	1.5	445 ± 10	1.0×10^{-5}	Radovic *et al.* (2002)

a Note these results are not valid for stresses less than 70 MPa.

resulting in large internal stresses. As the internal stresses increase, the creep rate decreases, leading to a quasi-steady-state. If the rate at which these stresses accrue is significantly higher than the rate at which they can relax, failure is brittle, insensitive to strain rate, and a function of grain size (Radovic *et al.* 2002). At the lowest strain rates and/or highest temperatures, the internal stresses can be accommodated by interlaminar decohesion, grain bending or kinking, and/or grain boundary decohesion and sliding. As the number of cavities and cracks increase and coalesce, this naturally leads to an increase in $\dot{\varepsilon}_{min}$ and a transition from secondary to tertiary creep. In other words, dislocation creep gives way to subcritical crack growth rate (Radovic *et al.* 2003, Zhen *et al.* 2004b).

To put it most succinctly, the response of the MAX phases to stress at elevated temperatures is directly related to the rate at which the internal stresses are relaxed (Radovic *et al.* 2000, 2001, 2002, 2003).

4. Solid Solution Hardening and Softening

Since substitutions can be made on either of the three sites in the MAX phases, the number of solid solutions possible is quite high. It is thus not unreasonable to assume that once the effects such substitutions have on the mechanical properties are understood, major improvements will accrue. Very little work exists on $M_{n+1}AX_n$ phase solid solutions, but what little exists is intriguing. Based on a limited dataset, it appears that *only* substitutions on the X-sites have a dramatic effect on properties. Substitutions on the M-sites (e.g., $(Ti_{0.5},Nb_{0.5})_2AlC$; Salama *et al.* 2002) or A-sites (e.g., $Ti_3(Si_{0.5},Ge_{0.5})C_2$; Ganguly *et al.* 2004) do not result in solid solution hardening. In contradistinction, the solid solution, $Ti_2AlC_{0.5}N_{0.5}$, is harder, more brittle, and significantly stronger, than the end-members Ti_2AlC and Ti_2AlN, which can be deformed plastically up to 5% strain even at room temperature (Barsoum *et al.* 2000). Interestingly, at temperatures $\approx$1200 °C a solid solution softening effect is observed, the reasons for which are still unclear, but could be related to the aforementioned interlaminar decohesions.

5. Tribological Properties and Machinability

As early as 1996 (Barsoum and El-Raghy 1996), it was noted that Ti_3SiC_2 shavings had a graphitic feel to them. This was later confirmed (Myhra *et al.* 1999, Crossley *et al.* 1999) when the friction coefficient, μ, of the basal planes of Ti_3SiC_2 was measured by lateral force microscopy and found, at $(2–5) \times 10^{-3}$ to be one of the lowest ever reported. Not only was this value exceptionally low, but it remained that low for up to 6 months exposure to the atmosphere. Unfortunately, this low friction coefficient does not translate to low friction in polycrystalline samples (El-Raghy *et al.* 2000). More recent results (Souchet *et al.* 2003), however, suggest that it may be possible to obtain surfaces with μ's against steel and Si_3N_4 as low as 0.15, especially at low stresses. More work, however, needs to be carried out to better understand and ultimately exploit this important property.

Lastly, one would be remiss not to mention probably the most characteristic trait of the MAX phases and one that truly sets them apart from other structural ceramics or high-temperature alloys: ease of machinability (Barsoum and El-Raghy 1996, 1997, Barsoum *et al.* 1997). The MAX phases are quite readily machinable with regular high-speed tool steels or even manual hacksaw. It is important to note that the machining does not occur by plastic deformation, as in the case of metals, but rather by the breaking off of tiny microscopic flakes. In that respect, they are not unlike other machinable ceramics such as Maycor™. The analogy with ice is also apt (Barsoum *et al.* 2001b); the $M_{n+1}AX_n$ compounds do not machine as one scoops ice cream (as in metals), but rather as in shaving ice. The MAX phases have some of the highest specific stiffnesses for readily machinable solids, with the exception of Be and Be alloys.

6. Summary and Conclusions

In a relatively short time, our understanding of the mechanical properties of these potentially technologically important materials has deepened considerably. This can be traced to two factors. First, the realization that the properties of these materials have a lot in common with two of the most widely studied materials: ice and graphite. The more recent realization that the MAX phases are part of a much larger class of solids—KNE solids (Barsoum *et al*. 2004a)—that is quite ubiquitous in nature and includes ice, graphite, layered oxides and silicates, nonlinear mesoscopic solids, NMEs (Guyer *et al*. 1995), and many more will indubitably result in even more rapid and deeper understanding. A sufficient condition to belong to this class of solids is plastic anisotropy and the absence of twinning, both almost guaranteed if the solid has a high c/a ratio (Barsoum *et al*. 2004a).

Second, and more important, must be the confinement of the dislocations to basal planes and the absence of twinning, which greatly simplifies the problem. Even in the unlikely eventuality that the MAX phases do not blossom into new applications, their study should greatly enhance our understanding of plastic deformation in other solids. These polycrystalline nanolaminates are almost ideal model materials for the study of dislocation dynamics and interactions of walls or pile-ups with grain boundaries, and other obstacles, without complicating factors, such a twinning, work hardening, formation of dislocations forests, etc., that have dogged metallurgists and material scientists almost from the inception of the field. The further prospect of studying dislocation dynamics in more than 50 MAX phases that exist, and the innumerable combinations of solid solutions, is a wonderful one indeed, and one that should prove to be of immense importance and benefit.

Acknowledgments

The progress made in understanding the mechanical properties of the MAX phases in a relatively short time is a testament to the graduate students, post-docs, and collaborators around the world, who have worked on these solids over the years. Foremost amongst them is Dr. T. El-Raghy, who was the first to study these phases and whose enthusiasm and productivity were contagious. A. Procopio, L. Ho-Duc, I. Salama, A. Murugaiah, T. Zhen and A. Ganguly, and Drs. L. Farber, N. Tzenov, and P. Finkel of Drexel University have also contributed much to our understanding of their mechanical properties. Without the support of Drs. D. Stepp of the Army Research Office, L. Madsen and L. Schioler of the Division of Materials Research of the NSF the progress outlined herein would not have been possible. My many excellent discussions with my colleagues at Drexel University—R. Doherty, S. Kalidindi, Y. Gogotsi, and A. Zavailangos—have also been invaluable.

Bibliography

Ashby M F 1989 On the engineering properties of materials. *Acta Metall.* **37**, 1273–93

Barsoum M W 2000 The $M_{n+1}AX_n$ phases: a new class of solids: thermodynamically stable nanolaminates. *Prog. Solid State Chem.* **28**, 201–81

Barsoum M W, El-Raghy T 1996 Synthesis and characterization of a remarkable ceramic: Ti_3SiC_2. *J. Amer. Cer. Soc.* **79**, 1953–6

Barsoum M W, El-Raghy T 1997 A progress report on Ti_3SiC_2, Ti_3GeC_2 and the H-phases, M_2BX. *J. Mater. Synth. Process.* **5**, 197–216

Barsoum M W, El-Raghy T 1999 Room temperature ductile carbides. *Met. Mater. Trans.* **30A**, 363–9

Barsoum M W, El-Raghy T 2001a The MAX phases: unique new carbide and nitride materials. *Am. Scientist* **89**, 336–45

Barsoum M W, Brodkin D, El-Raghy T 1997 Layered machinable ceramics for high temperature applications. *Scrip. Met. et. Mater.* **36**, 535–41

Barsoum M W, Farber L, Levin I, Procopio A, El-Raghy T, Berner A 1999a HRTEM of Ti_4AlN_3; or $Ti_3Al_2N_2$ revisited. *J. Amer. Cer. Soc.* **82**, 2545–7

Barsoum M W, Farber L, El-Raghy T, Levin I 1999b Dislocations, kink bands and room temperature plasticity of Ti_3SiC_2. *Met. Mater. Trans.* **30A**, 1727–38

Barsoum M W, Ali M, El-Raghy T 2000 Processing and characterization of Ti_2AlC, Ti_2AlN and $Ti_2AlC_{0.5}N_{0.5}$. *Met. Mater. Trans.* **31A**, 1857–65

Barsoum M W, Radovic M, Finkel P, El-Raghy T 2001b Ti_3SiC_2 and ice. *Appl. Phys. Lett.* **79**, 479–81

Barsoum M W, Zhen T, Kalidindi S, Radovic M, Murugaiah A 2003 Fully reversible, dislocation-based compressive deformation of Ti_3SiC_2 up to 1 GPa. *Nature Mater.* **2**, 107–11

Barsoum M W, Murugaiah A, Kalidindi S, Gogotsi Y 2004a Nanoindentations and kink bands in single crystal graphite. *Carbon* (in press)

Barsoum M W, Murugaiah A, Kalidindi S R, Zhen T 2004b Kinking nonlinear elastic solids, nanoidentations and geology (submitted for publication)

Chen I, Shirato K, Barsoum M W, El-Raghy T, Ritchie R O 2001 High-temperature cyclic fatigue-crack growth in monolithic Ti_3SiC_2 ceramics. *J. Amer. Cer. Soc.* **84**, 2914

Crossley A, Kisi E H, Summers J W B, Myhra S 1999 Ultra-low friction for a layered carbide-derived ceramic Ti_3SiC_2, investigated by lateral force microscopy. *J. Appl. Phys. D, Appl. Phys.* **32**, 632–8

Duval P, Ashby M F, Anderson I 1983 Rate-controlling processes in the creep of polycrystalline ice. *J. Phys. Chem.* **87**, 4066–74

El-Raghy T, Barsoum M W 1999 Processing and mechanical properties of Ti_3SiC_2: Part I. Reaction path and microstructure evolution. *J. Amer. Cer. Soc.* **82**, 2849–54

El-Raghy T, Zavaliangos A, Barsoum M W, Kalidindi S 1997 Damage mechanisms around hardness indentations in Ti_3SiC_2. *J. Amer. Cer. Soc.* **80**, 513–16

El-Raghy T, Barsoum M W, Zavaliangos A, Kalidindi S 1999 Processing and mechanical properties of Ti_3SiC_2: Part II. Mechanical properties. *J. Amer. Cer. Soc.* 2855–9

El-Raghy T, Blau P, Barsoum M W 2000 Effect of grain size on friction and wear behavior of Ti_3SiC_2. *Wear* **238**, 125–30

Farber L, Barsoum M W, Zavaliangos A, El-Raghy T, Levin I 1998 Dislocations and stacking faults in Ti_3SiC_2. *J. Amer. Cer. Soc.* **81**, 1677–81

Farber L, Levin I, Barsoum M W 1999 HRTEM study of a low-angle boundary in plastically deformed Ti_3SiC_2. *Phil. Mag. Lett.* **79**, 163

Frank F C, Stroh A N 1952 On the theory of kinking. *Proc. Phys. Soc.* **65**, 811–21

Ganguly A, Zhen T, Barsoum M W 2004 Synthesis and mechanical properties of $Ti_3(Si_xGe_{1-x})C_2$ ($x = 0$, 0.25, 0.5) solid solutions. *J. Alloys Compnds.* (in press)

Gilbert J, Bloyer D R, Barsoum M W, El-Raghy T, Tomsia A P, Ritchie R O 2000 Fatigue-crack growth and fracture properties of coarse and fine-grained Ti_3SiC_2. *Scrip. Mater.* **42**, 761–7

Goto T, Hirai T 1987 Chemically vapor deposited Ti_3SiC_2. *Mat. Res. Bull.* **22**, 1195–201.

Guyer R A, McCall K R, Boitnott G N 1995 Hysteresis, discrete memory and non-linear wave propagation in rock: a new paradigm. *Phys. Rev. Lett.* **74**, 3491

Hess J B, Barrett C S 1949 Structure and nature of kink bands in zinc. *Trans. AIME* **185**, 599–605

Holm B, Ahuja R, Johansson B 2001 *Ab initio* calculations of the mechanical properties of Ti_3SiC_2. *Appl. Phys. Lett.* **79**, 1450

Jeitschko W, Nowotny H 1967 Die Kristallstructur von Ti_3SiC_2—Ein Neuer Komplxcarbid-Typ. *Monatsh. fur Chem.* **98**, 329–37

Kooi A J, Poppen R J, Carvalho N J M, Th J, De Hosson M, Barsoum M W 2003 Ti_3SiC_2: a damage tolerant ceramic studied with nano-indentations and transmission electron microscopy. *Acta Mater.* **51**, 2859–72

Kuroda Y, Low I M, Barsoum M W, El-Raghy T 2001 Indentation responses and damage characteristics of hot isostatically pressed Ti_3SiC_2. *J. Aust. Ceram. Soc.* **37**, 95–102

Molina-Aldareguia J M, Emmerlich J, Palmquist J, Jansson U, Hultman L 2003 Kink formation around indents in laminated Ti_3SiC_2 thin-films studied in the nanoscale. *Scrip. Mater.* **49**, 155–60

Murugaiah A, Barsoum MW, Kalidindi S, Zhen T 2004 Spherical nanoindentations in Ti_3SiC_2, *J. Mater. Res.* (in press)

Myhra S, Summers J W B, Kisi E H 1999 Ti_3SiC_2—a layered ceramic exhibiting ultra-low friction. *Mater. Lett.* **39**, 6–11

Nickl J J, Schweitzer K K, Luxenberg P 1972 Gasphase-nabscheidung im systeme Ti–C–Si. *J. Less Common Metals* **26**, 335–53

Nowotny H 1970 Struktuchemie Einiger Verbindungen der Ubergangsmetalle mit den elementen C, Si, Ge, Sn. In: Reiss H (ed.) *Prog. Solid State Chem.* p. 27

Orowan E 1942 A type of plastic deformation new in metals. *Nature* **149**, 463–4

Pampuch R, Lis J, Stobierski L, Tymkiewicz M 1989 Solid combustion synthesis of Ti_3SiC_2. *J. Eur. Ceram. Soc.* **5**, 283

Pampuch R, Lis J, Piekarczyk J, Stobierski L 1993 Ti_3SiC_2-based materials produced by self-propagating high temperature synthesis and ceramic processing. *J. Mater. Synth. Process.* **1**, 93

Pietzka M A, Schuster J C 1994 Summary of constitution data of the system Al–C–Ti. *J. Phase Equilibria* **15**, 392–400

Procopio A T, Barsoum M W, El-Raghy T 2000 Characterization of Ti_4AlN_3. *Met. Mater. Trans.* **31A**, 333

Radovic M, Barsoum M W, El-Raghy T, Seidensticker J, Wiederhorn S 2000 Tensile properties of Ti_3SiC_2 in the 25–1300 °C temperature range. *Acta Mater.* **48**, 453–9

Radovic M, Barsoum M W, El-Raghy T, Wiederhorn S 2001 Tensile creep of fine-grained (3–5 μm) Ti_3SiC_2 in the 1000–1200 °C temperature range. *Acta Mater.* **49**, 4103–12

Radovic M, Barsoum M W, El-Raghy T, Wiederhorn S, Luecke W 2002 Effect of temperature, strain rate and grain size on the mechanical response of Ti_3SiC_2 in tension. *Acta Mater.* **50**, 1297–306

Radovic M, Barsoum M W, El-Raghy T, Wiederhorn S 2003 Tensile creep of coarse-grained (100–300 μm) Ti_3SiC_2 in the 1000–1200 °C temperature range. *J. Alloy. Compnds.* **361**, 299–312

Rawn C J, Barsoum M W, El-Raghy T, Procopio A, Hoffmann C M 2000 Structure of Ti_4AlN_{3-x}. *Mater. Res. Bull.* **35**, 1785–96

Salama I, El-Raghy T, Barsoum M W 2002 Synthesis and mechanical properties of Nb_2AlC and $(Ti,Nb)_2AlC$. *J. Alloys Compnds.* **347**, 271–8

Souchet A, Fontaine J, Belin M, Le Mogne T, Loubet J-L, Barsoum M W Dual Tribological Behavior of a Nanolayered Ceramic: Ti_3SiC_2. *Proc. of Spring* 2003 *MRS Conference, San Francisco, CA*

Stroh A N 1954 The formation of cracks as a result of plastic flow. *Proc. Roy. Soc. Lond. A* **223**, 404–14.

Stroh A N 1958 The cleavage of metal single crystals. *Phil. Mag.* **3**, 597–606

Tzenov N, Barsoum M W 2000 Synthesis and characterization of $Ti_3AlC_{1.8}$. *J. Amer. Cer. Soc.* **83**, 825–32

Wolfsgruber H, Nowotny H, Benesovsky F 1967 Die Kristallstuktur von Ti_3GeC_2. *Monatsh. Chem.* **98**, 2401

Yu R, Zhang Q, He L L, Zhou Y C, Ye H Q 2003 Stacking faults and grain boundaries of Ti_3SiC_2. *Phil. Mag.* **83**, 325–31

Zhen T, Barsoum M W, Kalidindi S R 2004a Compressive behavior of Ti_3SiC_2 at room and elevated temperatures (submitted for publication)

Zhen T, Barsoum M W, Kalidindi S R 2004b Compressive creep of Ti_3SiC_2 in the 1100–1300 °C temperature range in air (submitted for publication)

M. W. Barsoum and M. Radovic

Encyclopedia of Materials: Science and Technology
ISBN: 0-08-043152-6
pp. 1–16